

SPECTRAL RESPONSE OF THE EPIC-PN DETECTOR: BASIC DEPENDENCES

F. Haberl, U.G. Briel, K. Dennerl, and V.E. Zavlin

Max-Planck-Institut für extraterrestrische Physik, Giessenbachstraße 1, 85748 Garching, Germany

ABSTRACT

One of the three cameras behind the X-ray telescopes on board XMM-Newton is equipped with a pn CCD detector. Here the current status of the pn spectral response calibration is summarized. Several parameters describing the spectral response of the EPIC-pn detector show spatial dependencies. E.g. spectral resolution and single- to double-pixel event ratios are functions of the charge transfer losses and therefore depend on the distance to the read-out node of the CCD (the RAWY detector coordinate).

Key words: Missions: XMM-Newton – Instruments: EPIC-pn – Instruments: calibration

1. INTRODUCTION

On December 10, 1999 the XMM-Newton X-ray observatory (Jansen et al. 2001) was launched into a 48 h Earth orbit by an ARIANE V rocket. One of the three European Photon Imaging Cameras (EPIC, Turner et al. 2001) is equipped with a CCD detector based on pn technology (Strüder et al. 2001). Ground measurements and modeling of the spectral detector response of the EPIC-pn camera are described in Popp et al. (1999) and first results on the in-orbit performance of the EPIC-pn camera are presented in Briel et al. (2000). The current status of the EPIC-pn calibration is reported by Briel et al. (2002) in these conference proceedings.

2. SPECTRAL RESPONSE OF THE PN-CCD DETECTOR

The spectral detector response matrix (DRM) describes the detection probability for an X-ray photon with given energy in each of the 4096 ADU channels of the pn detector. The response to X-rays is calculated using the Partial Event Model (PEM) which is based on the charge collection function (Popp et al. 1999).

2.1. ENERGY DEPENDENCE

The PEM accounts for the effects of incomplete charge collection when photons are absorbed close to the detector

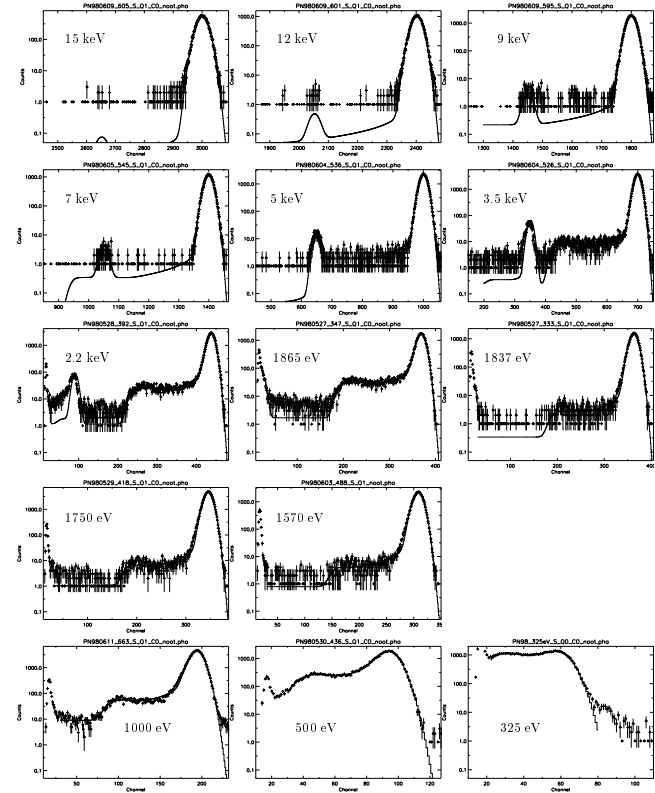


Figure 1. Spectral response to monochromatic radiation for 14 different energies as measured at the IAS synchrotron facility in Orsay, France, using the spare detector module (FM1). The spectra are averaged over CCD0 of quadrant 1 and shown with logarithmic intensity scale. The shoulder and flat shelf at the low energy side of the main peak are visible. Note the jump in shoulder height at the Si edge. At higher energies the Si escape peak is also visible.

surface. Different processes are responsible for the different spectral features that are visible in the measured spectrum. Figure 1 shows the spectral response to monochromatic X-rays for various photon energies. Absorption in the surface oxide causes detection of very few electrons that make it over the Si - SiO₂ boundary, resulting in a flat shelf that extends down to the noise peak (e.g. clearly visible in the 1 keV spectrum). If the photon is absorbed in the Silicon, but close to the Si surface, only a part of the generated electrons will reach the read-out node and

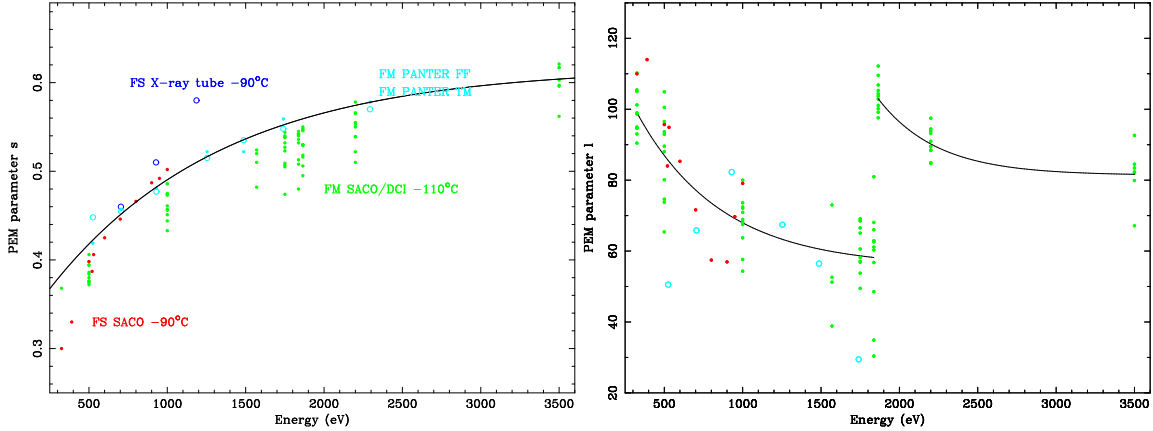


Figure 2. PEM parameters s and l which describe the shape of the low-energy shoulder as function of energy. The lines define best fit functions used in the DRM generation for the interpolation between energies.

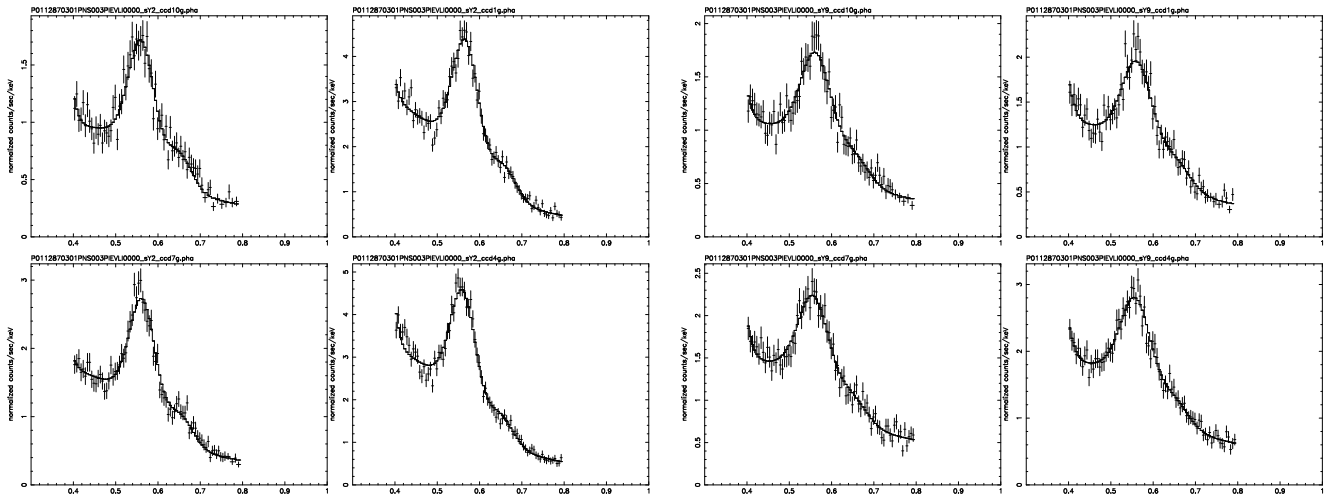


Figure 3. EPIC-pn spectra as function of channel energy (keV) obtained from extended fullframe mode observations of the Vela SNR. The large extent of the SNR and the soft spectrum with the dominating OVII He α line triplet allows to investigate spatial dependences of the spectral response at low energies. Spectra were selected from CCD lines (RAWY) 20-79 (left) and from lines 180-199 (right) for the inner four CCDs using single-pixel events. The OVII line blend is broader at larger distances to the read-out node.

a shoulder in the spectrum is produced. If the absorption takes place deep in the detector, all generated electrons will be detected. Since the absorption depth generally increases with energy the surface effects play a minor role at high energies (see e.g. the spectra from energies above 7 keV) and the response resembles a Gaussian peak with a width defined by the total detector noise (Fano, charge transfer and electronic noise).

The ground calibration spectra were used to derive the parameters for the PEM. Figure 2 shows the energy dependence of the s and l parameters. The PEM parameter s describes the minimum fraction of electrons which are detected when the photon is absorbed in the Si and is a direct measure for the low energy “end” of the shoulder. The parameter l is a characteristic length scale for the depth of the transition region near the surface of the de-

tor where the charge collection function changes from minimum s to full charge collection of 1 which is typically reached after 50-100 nm. The parameter l determines the height of the shoulder.

2.2. ENERGY RESOLUTION

The energy resolution of the detector is given by statistical processes in the charge production due to photo absorption, in the charge transfer during read-out and in the detector electronics. The charge transfer inefficiency (CTI), caused by traps in the Silicon which capture electrons, its modeling and correction is explained in detail in Dennerl et al. (2002) in these conference proceedings. Although the CTI losses can be corrected for, they introduce a noise component which influences the energy resolution.

This noise increases with distance of the detector pixel in which the photon is recorded to the read-out node (the RAWY detector coordinate). Figure 3 illustrates the degrading energy resolution with increasing RAWY distance on spectra obtained in orbit.

The energy resolution in terms of FWHM was derived directly from the current version of the response matrix by determining the width of the main spectral peak (for given photon energy) at half of the maximum intensity. Figure 4 shows the FWHM in eV as function of energy for five different line regions in the detector.

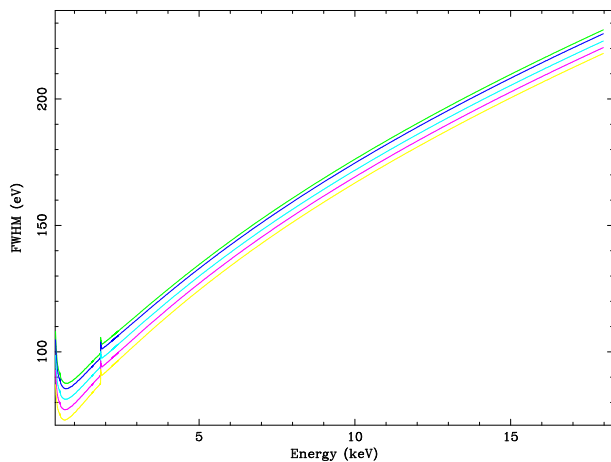


Figure 4. Spectral resolution of the EPIC-pn (single-pixel events) detector vs. energy for five line (RAWY) regions with different distance to the read-out node. Y1 (bottom curve, yellow) denotes RAWY=20-39, Y3 RAWY=60-79, Y5 RAWY=100-119, Y7 RAWY=140-159 and Y9 (upper curve, green) RAWY=180-199. The jump of the shoulder height (PEM parameter l) at the Si edge is reflected in the resolution. At the lowest energies the shoulder dominates the spectrum.

2.3. SINGLE- AND DOUBLE-PIXEL EVENTS

In the majority of cases an X-ray photon produces an electron cloud which is confined to a single detector pixel. However in cases where the photon is absorbed close to a pixel border the charge is split between two or more pixels (at most four in the case of the pn detector with its square pixel size of $150 \mu\text{m}$), producing double-, triple- and quadruple-pixel events. Because of the increasing size of the electron cloud at higher X-ray photon energies, the fraction of higher order events increases with energy. In the upper panels of Figure 5 two examples of pn spectra are shown. For each of the four valid event patterns a spectrum was binned. Double-event spectra start at higher PI channels (corrected for CTI losses) because to be recorded as “double” both events must exceed the electronic low-energy event threshold at the read-out node (which is cur-

rently set to 20 adu for the imaging modes and nominally 40 for timing mode). In a similar way this holds for “triples” and “quadruples”. In the lower panels of Figure 5 the relative fractions of the four valid event types normalized to their sum are plotted as function of energy. For the reason described above the single-fraction is 1.0 up to twice the threshold where doubles become detectable. However a small fraction of these singles are so-called pseudo singles, in reality doubles for which one of the two split partners fell below the event threshold. A further complication is the RAWY dependence of the event threshold. The fixed value defined in the electronics translates into effective thresholds which increase with distance to the read-out node due to CTI losses. An event which produces charge just above the threshold can fall below after the charge transport. This is demonstrated in Figure 5 for spectra taken closer to the read-out node (left) and near the detector center (right). Clearly seen is the start of the double spectrum at higher PI values in the latter case.

Comparison of single and double fractions derived from in-orbit data have shown that they are independent of source spectrum and source intensity as long as the spectrum is free of pile-up. This allows to derive standard curves for single- and double- fractions (triples and quadruples are neglected for spectral analysis due to their much reduced spectral resolution and small fractions) for each read-out mode. At higher intensities so called pattern pile-up increases the double fraction due to the production of false double-pixel events which actually consist of two neighboring single-pixel events. These false doubles cause deviations in the single and double fractions at PI channels typically twice the channels where the spectrum has its intensity maximum (there the probability for pile-up is highest). Examples are presented by Briel et al. (2002) and Haberl et al. (2002) in these proceedings.

A different kind of deviation from the standard curves at low PI channels can occur when the detector noise during an observation is at unusually high levels or when a spectrum is extracted from a region close to the read-out node where this noise is enhanced. A high level of low energy noise can result in an increased number of doubles, i.e. a noise peak in doubles is created at twice the energy of the noise seen in singles. This noise peak strongly increases the fraction of doubles just above twice the threshold (and correspondingly decreases the relative number of singles) as seen in Figure 5 by the deviations of the fractions at low energies from the expected curves. For a spectral analysis only energies above this double noise peak should be used and it is therefore recommended to produce pattern statistic plots from the events in the source extraction region.

The dependence of the effective event threshold and therefore the single and double fractions on RAWY is demonstrated in more detail in Figure 6 by plotting the

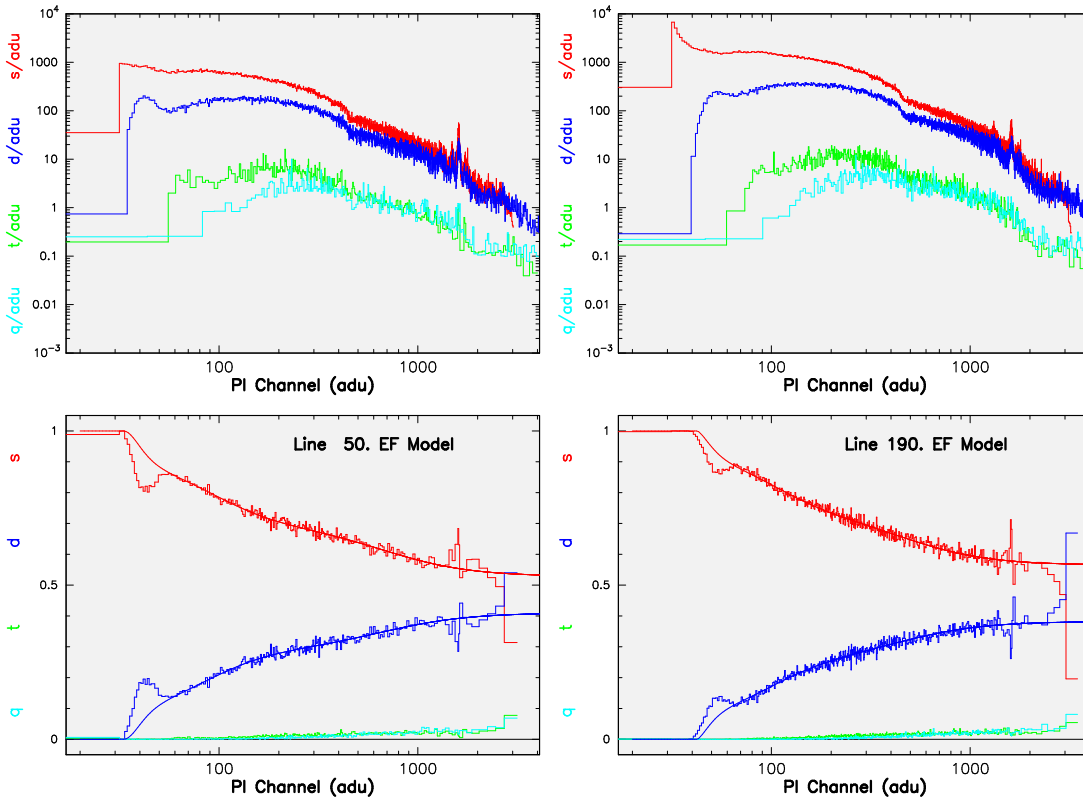


Figure 5. EPIC-pn spectra of single-, double-, triple-, and quadruple-events plotted as histograms (upper panels). The spectra were obtained from combined Coma observations in extended fullframe mode. In the lower panels the relative fractions of the different event types are shown vs. CTI-corrected PI channels. On the left spectra were selected from RAWY=40-59, on the right from RAWY=180-199. Note the increasing effective event threshold with increasing RAWY. The SAS task `epatplot` is available to produce these plots.

standard curves derived from areas with different distance to the read-out node (CAMEX).

ACKNOWLEDGEMENTS

The XMM-Newton project is an ESA Science Mission with instruments and contributions directly funded by ESA Member States and the USA (NASA). The XMM-Newton project is supported by the Bundesministerium für Bildung und Forschung / Deutsches Zentrum für Luft- und Raumfahrt (BMBF / DLR), the Max-Planck-Gesellschaft and the Heidenhain-Stiftung.

REFERENCES

- Briel U.G., Aschenbach B., Balasini M., et al. 2000, SPIE 4012, 154
 Briel U.G., Dennerl K., Freyberg M., et al. 2002, ESA SP-488, these proceedings
 Dennerl K., Briel U.G., Freyberg M., Haberl F., Meidinger N., Zavlin V.E. 2002, ESA SP-488, these proceedings
 Haberl F., Bennie P.J., Briel U.G., et al. 2002, ESA SP-488, these proceedings
 Jansen F., Lumb D., Altieri B., et al. 2001, A&A 365, L1
 Popp M., Haberl F., Briel U.G., Soltau H., Strüder L., 1999, SPIE 3765, 693

- Strüder L., Briel U., Dennerl K., et al. 2001, A&A 365, L18
 Turner M.J.L., Abbey A., Arnaud M., et al. 2001, A&A 365, L27

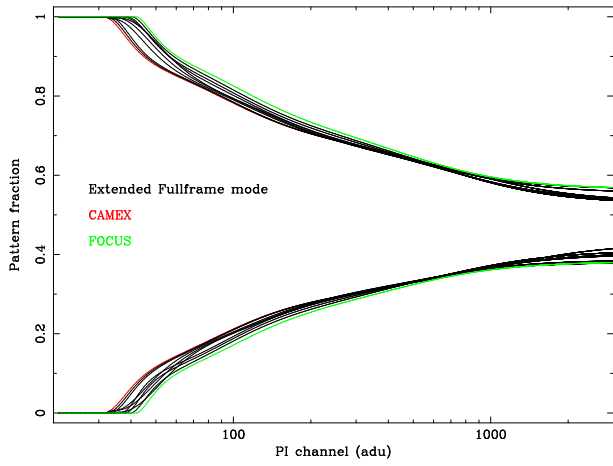


Figure 6. Standard curves for single (upper lines) and double fractions. Each line was obtained from spectra with different RAWY detector coordinates. Shown are ten curves from Y0: RAWY=0-19 (CAMEX) to Y9: RAWY=180-199.